Optimization of a solar-powered adsorptive ice-maker by a mathematical method

Optimization of a solar-powered adsorptive ice-maker by a mathematical method

A. Freni[a*], G. Maggio[a], S. Vasta[a], G. Santori[b], F. Polonara[b], G. Restuccia[a]

[a]*CNR - Istituto di Tecnologie Avanzate per l'Energia "Nicola Giordano",*

Via Salita S. Lucia sopra Contesse 5, 98126 Santa Lucia, Messina, Italy.

[b] *Università Politecnica delle Marche, Facoltà di Ingegneria, Dipartimento di Energetica,*

Via Brecce Bianche, Monte Dago, 60131 Ancona, Italy.

Abstract

In this paper, the simulation results of an adsorptive system driven by solar energy, to be used for freezing and cold storage, are presented. The system, consisting of an activated carbon reactor connected to a solar collector and to an evaporator/cold box, is able to produce and store 5 kg of ice/day, in a north Mediterranean climate. The simulations were carried out by a dynamic mathematical model which uses measured climatic data and that is based on energy balances of the components of the system. A parametric analysis, based on a Full Factorial Design (FFD) – a known statistical method used to evaluate the effects and interactions of different independent variables on a dependent variable – was accomplished. The results obtained evidenced that the most influencing parameters on the system performance are the transmittance/absorptivity coefficient of the solar collector and the heat transfer coefficient between the solar collector and the adsorbent material. Finally, the application of the Steepest Ascent Method (SAM) allowed to optimize the solar-powered adsorptive system, in terms of performance, and to determine the corresponding optimal values of the key parameters.

Keywords: Adsorption cooling, Solar ice-maker, Climatic data, Dynamic simulation, Full Factorial Design (FFD), Steepest Ascent Method (SAM).

* Corresponding author. Tel.: +39-90-624296; fax: +39-90-624247.
E-mail address: angelo.freni@itae.cnr.it (A. Freni).

Nomenclature

A_i (i=1-5, 9)	Heat transfer surface, m^2
c	Specific heat, J kg^{-1} K^{-1}
COPs	Solar Coefficient Of Performance
DIP	Daily Ice Production, kg
I_β	Available solar radiation @ β=30°, W m^{-2}
K_i (i=1-3)	Flag: 0 or 1 (see Tables 1-2 and Eq. 8)
L_a	Adsorbate latent heat of condensation/evaporation, J kg^{-1}
L_w	Water latent heat of solidification, J kg^{-1}
m	Mass, kg
m_a	Initial adsorbate mass inside the evaporator, kg
m_w	Liquid water mass, kg
n	Solar collector area, m^2
p	Pressure, Pa
T	Temperature, K
t	Time, s
t_{cycle}	Cycle time, s
UE	Useful effect, MJ
U_i (i=1-9)	Global heat transfer coefficient, W m^{-2} K^{-1}
U_α, U_β	Global heat transfer coefficients defined in Table 2, W m^{-2} K^{-1}
w	Uptake, kg kg^{-1}

Greek letters

$(\tau\alpha)_{eff}$	Transmittance/absorptivity coefficient
ΔH	Adsorption/desorption enthalpy, J kg^{-1}
ΔT	Variation of temperature, K
Δw	Variation of uptake, kg kg^{-1}

Subscripts

1	Solar collector/environment
2	Solar collector/adsorbent
3	Condenser/environment
4	Evaporator/liquid water
5	Environment/liquid water
6	Evaporator/phase-changing water
7	Evaporator/solid water
8	Environment/solid water
9	Evaporator/environment
a	Adsorbate
amb	Ambient
c	Condenser
eq	Equivalent
ev	Evaporator
ice	Iced water
lw	Liquid water
m	Solar collector
s	Solid adsorbent material (dry)
w	Water
β	Tilt angle

Superscripts

C	Closed ventilation windows
O	Open ventilation windows

1. Introduction

The solar-powered adsorptive systems are an efficient way to satisfy the cooling demand for air-conditioning, ice-making and medical or food storage in remote areas (Dieng and Wang, 2001). Indeed, such systems do not require electric energy, are noiseless and environmentally friendly. A specific application, proposed by many authors (Hu and Exell, 1994; Li and Sumathy, 1999; Anyanwu and Ezekwe, 2003), consists of a small size adsorbent reactor connected to a solar collector, for regeneration of the sorbent material during the day, and connected to an evaporator, for ice production during the night. The utilized adsorbent/adsorbate working pair is usually activated carbon/methanol. Different prototypes were realized, showing the potentiality of this technology (Sumathy and Zhongfu, 1998; Boubakri et al., 2000; Hildbrand et al., 2004). However, further development and optimization of the system design are required in order to produce compact, cheap and efficient units.

A mathematical model for simulation of a solar-powered adsorptive ice-maker has been presented in a previous work (Santori et al., 2006). The model was based on energy balances for the adsorbent reactor and the connected heat exchangers and allowed a description of the different phases of the thermodynamic cycle and the calculation of the performance in terms of Solar Coefficient Of Performance (*COPs*), Daily Ice Production (*DIP*) and Equivalent Daily Ice Production (DIP_{eq}). The simulation was performed for a whole year, using climatic data measured at the CNR-TAE Institute in Messina (38° 12' N, 15° 34' E), Italy. Results of simulation carried out on a base-case configuration of the solar-powered ice-maker, demonstrated that for a large part of the year (from April to October) a Daily Ice Production (*DIP*) of 5 kg can be obtained. The average annual *COPs* was 0.07. The obtained performance sounded attractive, but may be further improved. Consequently, aim of this work is to utilize the dynamic model in order to: a) carry out a parametric

analysis for assessment of the key-parameters of the system; b) optimize the design of the solar-powered ice-maker.

Results of the simulations are presented here in detail for a period of 20 days of May 2005. The parametric analysis is based on the Full Factorial Design (FFD) method (details can be found in Johnson and Leone, 1964; Box et al., 1978), while the system optimization is obtained by Steepest Ascent method (SAM) (see Miller et al., 1962; Box et al., 1978; Naik et al., 2004).

2. Description of the ice-maker

An adsorptive solar ice-maker consists of the following components: a solar collector, in which the adsorbent material (activated carbon) is embedded; a condenser for the adsorbate (methanol) condensation; a "cold chamber", containing the evaporator for the adsorbate and the liquid water to be frozen. A scheme is presented in Fig. 1.

The cycle is run through a day. During the daytime, the solar energy received by the collector allows the desorption of methanol from the sorbent bed. The methanol vapour flows to the condenser, condenses, and then is collected inside a receiver. The heat of condensation is released to the ambient; the uptake of refrigerant in the adsorbent reaches its minimum. During this time, all valves are closed (see Fig. 1). In the late afternoon the valve V_1 is opened, so that the liquid methanol flows from the receiver to the evaporator. Then, the valve V_1 is closed and the valve V_2 is opened for the whole night, allowing adsorption of methanol. The evaporation of methanol inside the cold chamber cools down the liquid water which is converted into ice.

From a thermodynamic point of view, the activated carbon/methanol working pair follows the classic adsorptive cycle made of four phases: I) isosteric heating; II) desorption at high temperature and pressure of condensation; III) isosteric cooling; IV) adsorption at low temperature and pressure of evaporation. Since the water may be at liquid phase, at solid/liquid mixture (phase-change) and at solid phase, Phase IV has been split into three corresponding steps.

More details on the thermodynamic cycle of adsorptive machines can be found elsewhere (Cacciola and Restuccia, 1995).

3. Modelling

The main assumptions of the model are the following:

- All components are spatially isothermal and isobaric. Thus, the temperature of the adsorbent material and those of the system components are considered only time-variable.
- The resistances to methanol diffusion, through the ice-maker components, are neglected.
- The adsorbent particles have uniform size, shape and distribution.
- The solid phase is in local thermal equilibrium with the gaseous phase.
- The gaseous phase behaves as an ideal gas.
- The thermal losses along the pipes are neglected.

The model governing equations are based on heat and mass balances for the components of the ice-maker.

Solar collector:

$$n(\tau\,\alpha)_{eff}\, I_{\beta} = m_m c_m \frac{dT_m}{dt} + U_2 A_2 (T_m - T_s) + U_1^{C/O} A_1 (T_m - T_{amb}) \tag{1}$$

Adsorbent bed:

$$U_2 A_2 (T_m - T_s) = (m_s c_s + w m_s c_a) \frac{dT_s}{dt} - K_1\, m_s \Delta H(w) \frac{dw}{dt} \tag{2}$$

Condenser:

$$L_a(T_c) m_s \frac{dw}{dt} = -m_c\, c_c \frac{dT_c}{dt} - U_3 A_3 (T_c - T_{amb}) \tag{3a}$$

Evaporator:

$$L_a(T_{ev}) m_s \frac{dw}{dt} = -U_{\alpha} A_4 (T_{ev} - T_w) - [m_{ev}\, c_{ev} + (m_a - \Delta w\, m_s) c_a] \frac{dT_{ev}}{dt} - U_9 A_9 (T_{ev} - T_{amb}) \tag{3b}$$

Heat and mass balances for water/ice:

$$m_w c_w \frac{dT_w}{dt} = U_\alpha A_4 \left(T_{ev} - T_w\right) + U_\beta A_5 \left(T_w - T_{amb}\right) \tag{4}$$

$$L_w \frac{dm_{ice}}{dt} = L_a \left(T_{ev}\right) m_s \frac{dw}{dt} \tag{5}$$

Further supplementary equations are reported in Appendix A.

The accompanying initial conditions and starting values are:

$$T_m(0) = T_s(0) = T_{amb}(0) \tag{6a}$$

$$p_s(0) = p_{ev} \tag{6b}$$

$$w(0) = w_2 \tag{6c}$$

$$T_c(t_1) = T_{amb}(t_1) \tag{7a}$$

$$T_{ev}(t_3) = T_w(t_3) = T_{ev,0} \tag{7b}$$

$$m_{ice}(t_{4a}) = 0 \tag{7c}$$

where p_{ev} is calculated from the initial evaporator temperature, w_2 is calculated from the initial temperature and pressure of the adsorber, t_1 is the time of the end of Phase I (and start of Phase II), t_3 is the time of the end of Phase III (and start of Step IVa), t_{4a} is the time of the end of Step IVa (and start of Step IVb) and $T_{ev,0}$ is the initial evaporator temperature.

Depending on the phase of the thermodynamic cycle described by the adsorptive ice-maker, only a certain number of the previous equations (1)-(5) is applied and the relative coefficients/parameters (K_1, $U_1^{C/O}$, U_α, U_β, c_w) assume a different form (see Tables 1-2).

Some details on the different phases are given below.

- *Phase I* (*isosteric heating*): The adsorbent is heated up along the upper isosteric curve, and the pressure increases from p_{ev} to p_c. The shift condition to the next phase is established when p_s=p_c, i.e. when the adsorbent bed pressure reaches the condenser pressure.

- *Phase II* (*desorption*): The adsorbent material releases the methanol to the condenser, so that, the uptake varies between the upper and the lower isosteric curve. The shift condition to the next phase is established when the useful solar radiation of the day drops below a certain value (I_β<100 W m^{-2}) or the methanol uptake is lower than 2%.
- *Phase III* (*isosteric cooling*): When one of the two above mentioned conditions occurs, the adsorbent bed is cooled down along the lower isosteric curve. The shift condition to the next phase is established when $p_s=p_{ev}$, i.e. when the adsorbent bed pressure reaches the evaporator pressure.
- *Phase IV* (*adsorption*): The adsorbent material adsorbs methanol from the evaporator, and the uptake varies from the lower to the upper isosteric curve. In the meantime, the methanol evaporation results in useful effect of water cooling. The water initial temperature (10 °C) decreases to 0 °C; then the liquid water undergoes a phase-change (ice) at constant temperature and finally it is under-cooled until the next day comes, or until the methanol contained in the evaporator is completely evaporated. Phase IV has been split into three steps, because the water may be at liquid phase (Step a), at solid/liquid mixture (Step b) and at solid phase (Step c).

Finally, for each day, the corresponding Solar Coefficient Of Performance (*COPs*) is calculated as:

$$COPs = \frac{Useful\ effect}{Available\ solar\ energy} = \frac{m_w\, c_{lw}\, \Delta T_w\big|_{step\ IVa} + K_2\, m_{ice}\, L_w + K_3\, m_w\, c_{ice}\, \Delta T_w\big|_{step\ IVc}}{n \int_0^{t_{cycle}} I_\beta(t)\, dt} \tag{8}$$

where K_2=0 and/or K_3=0 when Step IVb and/or IVc, respectively, does not occur.

The Daily Ice Production (*DIP*) and its equivalent value (DIP_{eq}), which accounts for the equivalent mass of ice corresponding to the under-cooling, are given by

$$DIP = K_2\, m_{ice} \tag{9a}$$

$$DIP_{eq} = DIP\left(1 + \frac{m_w\, c_{ice}\, \Delta T_w\big|_{step\ IVc}}{m_{ice}\, L_w}\right) \tag{9b}$$

The model equations were numerically solved by using the commercial software Mathematica® for ordinary differential equation (ODE) systems, based on a function which automatically switches between stiff (Gear) and non-stiff (Adams) integration methods (see Radhakrishnan and Hindmarsh, 1994).

4. Parametric study and optimization of the ice-maker design

4.1 Input data and considerations on climatic data

Main input data of the model are reported in Tab. 3. Fig. 2 shows, the values of the dynamic data (I_β and T_{amb}) for the considered twenty-day period (May 3-22, 2005). The weather data of May have been used in order to demonstrate that the ice-maker is able to efficiently work (high *DIP*) also in springtime, and not only during the hottest months.

Tab. 4 summarizes the corresponding statistical values of these parameters: minimum, maximum and average daily temperature; maximum and average daily solar radiation (calculated from sunrise to sunset). From this table results that the daily average ambient temperatures range from 15.4 °C to 19.1 °C; while the daily average useful solar radiation varies from 357 W m^{-2} to 673 W m^{-2}, with a maximum radiation ranging from 973 W m^{-2} to 1070 W m^{-2}. Minimum average temperatures occur on May 3 and May 9-10, whilst minimum average solar radiations on May 6 and May 13. In particular, May 3 and May 6 are characterised both by a low average temperature and a low average radiation.

Finally, it is worthy to mention that some days (May 5-6, May 8, and May 13-14) are characterised by very unstable climatic conditions (see Fig. 2); this, as discussed later, affects the results.

4.2 Parametric study by Full Factorial Design

A factorial design is a method to study the effect of two or more variables (factors) on a response variable (Johnson and Leone, 1964; Box et al., 1978). A fixed number of levels for each factor has to be selected to perform the factorial design. By considering k variables and two-levels, a full factorial design requires 2^k runs or experiments to be performed.

In this case a 2^4 Full Factorial Design (FFD) has been used to analyse the influence of some key parameters on the ice-maker model results. The investigated parameters are: the transmittance/absorptivity coefficient ($(\tau\alpha)_{eff}$), the mass of the solar collector (m_m), the global heat transfer coefficient between solar collector and adsorbent (U_2), and the heat transfer surface between evaporator and water (A_4). This choice is justified because the objective of this paper is not the optimization of the adsorber, but the optimization of the system. Therefore some parameters (e.g. the mass of adsorbent and the adsorber geometry) have been fixed; furthermore, instead of changing the solar collector surface – which would have involved a change of the values of several other parameters related to the ice-maker size – we preferred to modify the transmittance/absorptivity coefficient ($(\tau\alpha)_{eff}$), which depends only on the type of panel used.

The lower and upper levels of the key parameters are reported in Tab. 5. The 16 runs, with the corresponding values of the four parameters, are listed in Tab. 6; where are also reported the calculated values of the performance parameters: Solar Coefficient Of Performance (*COPs*), Useful Effect (*UE*), Daily Ice Production (*DIP*) and Equivalent Daily Ice Production (DIP_{eq}). It should be noted that this table reports the average values calculated over the 20-day period considered.

The *DIP* and *COPs* values derived from these model calculations are, respectively, in the order of 4.7-5.0 kg day^{-1} (i.e. 3.1-3.3 kg m^{-2} day^{-1}) and 0.04-0.05. These values are slightly lower than those reported in literature, as typical for ice-makers based on the activated carbon/methanol pair: *DIP*= 4-5 kg m^{-2} day^{-1} and *COPs*= 0.10-0.14 (e.g. Sumathy and Zhongfu, 1998; Li et al., 2002). Nevertheless, this is due to the climatic conditions of May; in fact, some further investigations (Santori et al., 2006) demonstrated that for winter months a *COPs* of 0.11 can be obtained, much

coherent with literature values. This represents a preliminary validation of the proposed model, which should be definitely accomplished when the measured performance parameters of a prototype will be available.

Fig. 3 shows that the average values of all the performance parameters (*COPs*, *UE*, *DIP* and DIP_{eq}) have similar qualitative behaviours. Therefore, the parametric study can be focused on a single parameter, the Equivalent Daily Ice Production, whose values, calculated for all the 20-days and all the 16 FFD runs, are presented in Fig. 4a,b.

Fig. 4a shows that if the transmittance/absorptivity coefficient is low (odd runs) the ice-maker is not always able to reach the targeted 5 kg of Daily Ice Production and, consequently, also the DIP_{eq} is lower than 5 kg. This result depends on the climatic conditions: in fact, low DIP_{eq} values (minimum 2.14 kg) occur when the average daily solar radiation is low and/or when there are large fluctuations on the daily radiation (May 3, May 5-6, May 14, 2005), independently of the average ambient temperature. For the same reason the DIP_{eq} value corresponding to May 8 and May 13 is only 5 kg. On the contrary, when the transmittance/absorptivity coefficient is high (even runs, Fig. 4b) the DIP_{eq} values are higher than 5.17 kg and the variations are less remarkable (maximum 5.65 kg).

Further information are given in Tab. 7 where the minimum, maximum and average values, calculated over the 20-day period for each run, are reported. As seen from this table, the largest value of the average DIP_{eq} (5.48 kg) has been obtained for the run #8, i.e. that with $(\tau\alpha)_{eff}$ =0.8, U_2=200 W m^{-2} K^{-1}, m_m=50 Kg and A_4=2 m^2. It must be also remarked that the other performance parameters calculated for this run, and reported in Tab. 6, are the highest of the 16 FFD runs.

Going on with the method, the estimated mean effects of each parameter (and their interactions) on the average DIP_{eq} were calculated using the Yate's algorithm (Miller et al., 1962; Box et al., 1978). This method is applied in Tab. 8, where column (2) contains the average DIP_{eq} values corresponding to each run of the design matrix of Tab. 6. These values are then considered in successive pairs, to obtain the entries in column (3): the first eight entries are obtained by adding the pairs together; while, the second eight entries are obtained by subtracting the *top number from the*

bottom number of each pair. The entries in columns (4) to (6) are obtained analogously from columns (3) to (5). Finally, the effects in column (8) are calculated by dividing the values of column (6) by the appropriate divisors shown in column (7). The first estimate is the grand average of all the runs; the remaining effects are identified on the basis of the plus signs in the design matrix.

They represent the mean variation of the DIP_{eq} value due to the change, from the lower to the upper level, of the single factors $(\tau\alpha)_{eff}$, m_m, U_2, A_4 (main effects) and the effects of multiple-factor interactions. To better evidence the respective importance, these effects are plotted in Fig. 5, where it is possible to recognize that the parameter that has the strongest influence on the DIP_{eq} is the transmittance/absorptivity coefficient (effect +0.55), followed in importance by the global solar collector/adsorbent heat transfer coefficient (effect +0.12). It can be observed that the main effects of both $(\tau\alpha)_{eff}$ and U_2 have a positive value. This means that DIP_{eq} increases when these parameters increase; while an increase of m_m or A_4 produces a negative effect (i.e. a decrease) on DIP_{eq}. Nevertheless, it should be remarked that the main effects of these two parameters (m_m and A_4) and all the multiple-factor interactions have a negligible influence, except for the two-factor interaction $(\tau\alpha)_{eff}\,U_2$; which has a negative effect (–0.10).

The simulation results evidenced that the sensible heat of the solar collector and the heat transfer surface between evaporator and water have a small role on the energy balances described by equations (1) and (3b). This is the reason of the less remarkable influence of m_m and A_4 on the DIP_{eq} values.

As suggested by Box et al. (1978), the nature of the interaction $(\tau\alpha)_{eff}\,U_2$ deserves to be better investigated by considering a two-way table. This is done in Fig. 6, where the lower and upper levels (denoted by – and + sign, respectively) of the two parameters $(\tau\alpha)_{eff}$ and U_2 are shown. At the four corners (labelled with *A*, *B*, *C* and *D*) there are the values obtained as the average of the FFD runs corresponding to the combinations of the two levels of these two key parameters.

Based on this two-way table, the main effects of $(\tau\alpha)_{eff}$ and U_2 and the interaction effect $(\tau\alpha)_{eff}\,U_2$ can be easily recalculated, respectively, as

$$Effect\ of\ (\tau\alpha)_{eff}:\ \frac{(B-A)+(C-D)}{2}=+0.55\,\text{kg}$$

$$Effect\ of\ U_2:\ \frac{(A-D)+(B-C)}{2}=+0.13\,\text{kg}$$

$$Effect\ of\ (\tau\alpha)_{eff}U_2:\ \frac{(B-C)-(A-D)}{2}=-0.10\,\text{kg}.$$

In general, a two-factor interaction can be interpreted as the total effect of a change of factor 1 from low to high level when factor 2 stays at high level, minus the same effect when factor 2 stays at low level. Therefore, in our case, the interaction effect $(\tau\alpha)_{eff}\,U_2$ resulted negative, because the variation of DIP_{eq} corresponding to the cases with $(\tau\alpha)_{eff}$=0.8 is less remarkable than the variation corresponding to the cases with $(\tau\alpha)_{eff}$=0.5. This leads to another important consideration: the influence of U_2 on DIP_{eq} is hidden by the effect of $(\tau\alpha)_{eff}$, especially for large values of the latter parameter (e.g. 0.8). On the contrary, the influence of U_2 can be better appreciated when $(\tau\alpha)_{eff}$ is as low as 0.5. Besides, the analysis allows us to exclude possible interaction effects that could "alter" the (main) effects of the single parameters $(\tau\alpha)_{eff}$ and U_2.

The order of importance of the parameters and, in general, the distribution of the (main and interaction) effects for DIP_{eq}, have also been confirmed for the other three performance parameters (i.e. *COPs*, *UE* and *DIP*).

4.3 Optimization by Steepest Ascent Method

The FFD gave us interesting information about the influence of the key parameters; besides, the best run resulting from the FFD corresponds to an average DIP_{eq} of 5.48 kg (Tab. 7, run #8), but this value and the related key parameters are not the optimal ones.

To this purpose, optimization of the system performance can be obtained by adoption of the Steepest Ascent Method (SAM), an iterative technique which involves moving trough an appropriate path that yields increases in the response (Miller et al., 1962; Box et al., 1978; Naik et al., 2004; Kowalski et al., 2005).

The SAM is applied in Tab. 9. The procedure starts with calculation of the mean levels of the key parameters of the FFD, that are considered as the base point of the SAM. A set of further runs is determined with a step which is proportional to the magnitude of the effects calculated by the FFD and acts in the direction of their signs. In particular, the increments Δz_j are obtained as the difference between the upper and mean levels; the coefficients b_j are the values of the effects of each parameter determined by the FFD. The magnitudes of the steps are obtained by dividing the product $\Delta z_j \; b_j$ by the maximum value of b_j. Then, the effective steps may be obtained by normalizing these magnitudes for a constant – in our case equal to 3 – in order to define a significant number of further runs to be investigated.

In this case, the obtained steps have been normalized in such a way to have a 0.05 increase of $(\tau\alpha)_{eff}$. This leads to the identification of five runs, labelled as SA1-SA5. It should also be remarked that the values of the two parameters m_m and A_4 have been fixed to 30 kg and 6 m^2, respectively. This because their influence is almost insignificant, as demonstrated by the results of the FFD, and confirmed by the negligible relative steps determined by the SAM.

The results of simulations corresponding to the SAM are shown in Tab. 10, where again only the DIP_{eq} values have been reported. As expected, passing from run SA1 to run SA5, there is an increase of the Equivalent Daily Ice Production, which reaches a daily maximum of 5.74 kg and an average of 5.57 kg (for the 20-day period considered) in the case of run SA5.

Therefore, the optimal values of the key parameters are the following: $(\tau\alpha)_{eff}$=0.9, U_2=139.2 W m^{-2} K^{-1}, m_m=30 kg and A_4=6 m^2. Besides, let us mention that the average values of the other performance parameters calculated for this run are: *COPs*=0.052, *UE*=2.07 MJ and *DIP*=5 kg.

The fact that the optimal value of $(\tau\alpha)_{eff}$ is higher than the maximum considered in the FFD (0.8) must not be surprising, because this is justified by the fact that the FFD – which gives only a preliminary indication of the effects – evidenced that this parameter is the most influencing one: this approach is also followed by other authors, e.g. Shukla et al. (1989). On the contrary, an increase of U_2 beyond 139.2 W m^{-2} K^{-1} will provide also an improvement of the system

performance but, as it can be expected (see Fig. 5), this would be essentially worthless compared to that obtained by increasing $(\tau\alpha)_{eff}$.

Finally, in Fig. 7 the dynamic behaviour of the adsorbent and condenser temperature, corresponding to the optimal case, is shown. This figure evidences that the maximum daily temperature reached by the activated carbon is about 110 °C (on May 12), with a lowest temperature of about 70 °C, due to the unfavourable climatic conditions of May 6. The condenser temperature was always slightly higher than the ambient temperature.

5. Conclusions

The parametric analysis and design optimization of a solar-powered adsorptive ice-maker was carried out using a predictive mathematical model. Application of 2^4 Full Factorial Design (FFD) method showed that the highest values of the average DIP_{eq} and $COPs$, obtained for the 20-day period considered (May 3-22, 2005), were respectively 5.48 kg and 0.051. Furthermore, the FFD made possible to assess that the two most influencing parameters on the system performance are the transmittance/absorptivity coefficient of the solar collector, $(\tau\alpha)_{eff}$, and the heat transfer coefficient between the solar collector and the adsorbent material, U_2. Finally, by the Steepest Ascent Method (SAM) the optimal values of the key parameters have been identified: $(\tau\alpha)_{eff}$=0.9, U_2=139.2 W m^{-2} K^{-1}, m_m=30 kg and A_4=6 m^2. The corresponding average DIP_{eq} is 5.57 kg.

Appendix A

- The adsorbent/adsorbate equilibrium was calculated by the following equation:

$$ln(p_s) = A(w) + \frac{B(w)}{T_s} \quad \textbf{(A1),}$$

where the terms $A(w)$ and $B(w)$ are polynomials

$$A(w) = a_0 + a_1\, w + a_2\, w^2 + a_3\, w^3 \quad \textbf{(A2),}$$

$$B(w) = b_0 + b_1\, w + b_2\, w^2 + b_3\, w^3 \qquad \textbf{(A3),}$$

whose coefficients are determined experimentally.

- The adsorption/desorption enthalpy $\Delta H(w)$ appearing in equation (2) was calculated as

$$\Delta H(w) = -B(w)\, R \qquad \textbf{(A4),}$$

where R is the gas constant for adsorbate, which is about 259.5 J $kg^{-1}K^{-1}$ for methanol.

- The condensation/evaporation pressure is given by

$$ln(p_c) = c_0 + \frac{c_1}{T_c} + \frac{c_2}{T_c^2} + \frac{c_3}{T_c^3} \qquad \textbf{(A5a),}$$

$$ln(p_{ev}) = c_0 + \frac{c_1}{T_{ev}} + \frac{c_2}{T_{ev}^2} + \frac{c_3}{T_{ev}^3} \qquad \textbf{(A5b).}$$

- The latent heat of condensation/evaporation of adsorbate, was calculated as a function of temperature by

$$L_a(T) = d_0 + d_1\, T + d_2\, T^2 + d_3\, T^3 \qquad \textbf{(A6).}$$

References

Anyanwu, E.E., Ezekwe, C.I., 2003. Design, construction and test run of a solid adsorption solar refrigerator using activated carbon/methanol, as adsorbent/adsorbate pair. Energy Conversion & Management 44, 2879-2892.

Boubakri, A., Guilleminot, J., Meunier, F., 2000. Adsorptive solar powered ice-maker: experiments and model. Solar Energy 69 (3), 249-263.

Box, G.E.P., Hunter, W.G., Hunter, J.S., 1978. Statistics for experimenters, Wiley, New York.

Cacciola, G., Restuccia, G., 1995. Reversible adsorption heat pump: a thermodynamic model. International Journal of Refrigeration 18 (2), 100-106.

Dieng, A., Wang, R.Z., 2001. Literature review on solar adsorption technologies for ice-making and air-conditioning purposes and recent developments in solar technology. Renewable & Sustainable Energy Reviews 5, 313-342.

Hildbrand, C., Dind, P., Pons, M., Buchter, F., 2004. A new solar powered adsorption refrigerator with high performance. Solar Energy 77 (3), 311-318.

Hu, E.J., Exell, R.H.B., 1994. Simulation and sensitivity analysis of an intermittent solar powered charcoal/methanol refrigerator. Renewable Energy 4 (1), 133-149

Johnson, N.L., Leone, F.C., 1964. Statistics and experimental design in engineering and the physical sciences, Vol. 2, Wiley, New York.

Kowalski, S.M., Borror, C.M., Montgomery, D.C., 2005. A modified path of steepest ascent for split-plot experiments. Journal of Quality Technology 37 (1), 75-83.

Li, Z.F., Sumathy, K., 1999. A solar powered ice-maker with the solid adsorption pair of activated carbon and methanol. International Journal of Energy Research 23, 517-527.

Li, M., Wang, R.Z., Xu, Y., Wu, J., Dieng, A., 2002. Experimental study on dynamic performance analysis of a flat-plate solar solid-adsorption refrigeration for ice maker. Renewable Energy 27, 211-21.

Miller, M.C., Biswell, H.A., Goaz, P.W., 1962. Application of the method of steepest ascent to the response surface of the nitrate-nitrite reductase activity in salivary sediment. Journal of Dental Research 41 (3), 549-572.

Naik, P.K., Reddy, P.S.R., Misra, V.N., 2004. Optimization of coal flotation using statistical technique. Fuel Processing Technology 85, 1473-1485.

Radhakrishnan, K., Hindmarsh, A.C., 1994. Description and Use of LSODE, the Livermore Solver for Ordinary Differential Equations. Lawrence Livermore National Laboratory technical report UCRL-ID-113855.

Santori, G., Vasta, S., Maggio, G., Freni, A., Polonara, F., Restuccia, G., 2006. Modelling and design of an adsorptive solar ice-maker. In: Conference Proceedings of the 61st ATI National Congress, International Session "Solar Heating and Cooling", Perugia, Italy, pp. 87-93.

Shukla, A.K., Stevens, P., Hamnett, A., Goodenough, J.B., 1989. A Nafion-bound platinized carbon electrode for oxygen reduction in solid polymer electrolyte cells. Journal of Applied Electrochemistry 19, 383-386.

Sumathy, K., Zhongfu, L., 1998. Experiments with solar-powered adsorption ice-maker. Renewable Energy 16, 704-707.

Table 1: Equations, Coefficients and End phase conditions for Phase I and III

	Phase I	Phase III
Equations	Eq. (1) Eq. (2) Eq. (A1)	
Coefficients	K_1=0	
	$U_1^{C/O} = U_1^C$	$U_1^{C/O} = U_1^O$
End phase condition	p_s=p_c	p_s=p_{ev}

Table 2: Equations, Coefficients and End phase conditions for Phase II and IV

	Phase II	Phase IV		
		Step a	Step b	Step c
Equations		Eq. (1) Eq. (2) Eq. (A1)		
	Eq. (3a) Eq. (A5a)		Eq. (3b) Eq. (A5b)	
		Eq. (4)	Eq. (5)	Eq. (4)
Coefficients		K_1=1		
	$U_1^{C/O} = U_1^C$		$U_1^{C/O} = U_1^O$	
		U_α=U_4, U_β=U_5, c_w=c_{lw}	U_α=U_6	U_α=U_7, U_β=U_8, c_w=c_{ice}
End phase condition	I_β<100 $W\ m^{-2}$ *or* $w \leq 2\%$	T_w=0 or *t= 24 h*	m_{ice}=m_w or *t= 24 h*	*t= 24 h*

Table 3: Main model input data (see nomenclature for definitions).

n=1.5 m^2	$T_{ev,0}$=10 °C			
m_s=36 kg	m_c=5 kg	m_{ev}=10 kg	m_a=1.5 kg	m_w=5 kg
A_1=4.2 m^2	A_2=4.2 m^2	A_3=2 m^2	A_5=1 m^2	A_9=1 m^2
U_1^C =3 W m^{-2} K^{-1}	U_1^O =25 W m^{-2} K^{-1}	U_3=200 W m^{-2} K^{-1}	U_4=3000 W m^{-2} K^{-1}	U_5=0.2 W m^{-2} K^{-1}
U_6=100 W m^{-2} K^{-1}	U_7=10 W m^{-2} K^{-1}	U_8=0.1 W m^{-2} K^{-1}	U_9=1 W m^{-2} K^{-1}	

Table 4: Statistical values of temperature and radiation for May 2005

May 2005 day	***Ambient temperature* (°C)**			***Solar radiation* (W m^{-2})**	
	min	max	avg	max	avg*
3	15.1	18.3	16.7	1013	487
4	14.5	23.6	18.7	1031	546
5	15.1	23.1	17.9	973	477
6	13.6	22.3	16.8	991	357
7	13.9	21.7	17.0	1028	634
8	13.7	22.7	16.9	1017	456
9	13.8	17.5	15.4	1043	607
10	12.4	20.1	16.3	1070	673
11	15.3	23.1	17.4	1020	662
12	14.5	21.4	17.5	1021	604
13	15.5	20.4	17.1	1058	359
14	13.8	20.6	17.5	1011	446
15	14.0	21.5	17.7	1018	645
16	15.1	25.2	18.5	1061	642
17	12.5	21.6	17.2	1061	669
18	13.1	21.2	17.2	1041	654
19	16.2	23.8	18.8	1012	659
20	15.2	23.3	19.1	998	649
21	14.1	24.0	18.5	1025	642
22	14.7	20.1	17.8	1014	638

***** *The average solar radiation is calculated from sunrise to sunset.*

Table 5: Range of variation of the key parameters used for FFD

Symbol	***Definition***	***Range***
$(\tau\alpha)_{eff}$	Transmittance/absorptivity coefficient	0.5 – 0.8
m_m	Solar collector mass	10 – 50 kg
U_2	Global heat transfer coefficient solar collector/adsorbent	4 – 200 W m^{-2} K^{-1}
A_4	Heat transfer surface evaporator/water	2 – 10 m^2

Table 6: The 2^4 FFD and calculated average values of performance parameters

Run	Design matrix				$(\tau\alpha)_{eff}$	m_m (kg)	U_2 (W m^{-2} K^{-1})	A_4 (m^2)	Calculated values*			
									COPs	*UE* (MJ)	*DIP* (kg)	DIP_{eq} (kg)
1	–	–	–	–	0.5	10	4	2	0.044	1.81	4.71	4.80
2	+	–	–	–	0.8	10	4	2	0.051	2.03	5.00	5.45
3	–	+	–	–	0.5	50	4	2	0.044	1.81	4.71	4.80
4	+	+	–	–	0.8	50	4	2	0.051	2.03	5.00	5.45
5	–	–	+	–	0.5	10	200	2	0.047	1.90	4.93	5.04
6	+	–	+	–	0.8	10	200	2	0.051	2.04	5.00	5.47
7	–	+	+	–	0.5	50	200	2	0.047	1.89	4.92	5.03
8	+	+	+	–	0.8	50	200	2	0.051	2.04	5.00	5.48
9	–	–	–	+	0.5	10	4	10	0.044	1.81	4.71	4.79
10	+	–	–	+	0.8	10	4	10	0.051	2.03	5.00	5.44
11	–	+	–	+	0.5	50	4	10	0.044	1.81	4.71	4.79
12	+	+	–	+	0.8	50	4	10	0.051	2.03	5.00	5.44
13	–	–	+	+	0.5	10	200	10	0.047	1.89	4.92	5.02
14	+	–	+	+	0.8	10	200	10	0.051	2.03	5.00	5.46
15	–	+	+	+	0.5	50	200	10	0.047	1.88	4.90	5.00
16	+	+	+	+	0.8	50	200	10	0.051	2.04	5.00	5.46

** Average values for the 20-day period considered.*

Table 7: Minimum, maximum and average values of DIP_{eq} (kg) for FFD runs.

	Run number															
	1	**2**	**3**	**4**	**5**	**6**	**7**	**8**	**9**	**10**	**11**	**12**	**13**	**14**	**15**	**16**
min	2.26	5.21	2.18	5.22	3.59	5.21	3.31	5.21	2.23	5.20	2.14	5.20	3.32	5.18	3.05	5.17
max	5.23	5.61	5.23	5.62	5.30	5.63	5.29	5.65	5.22	5.60	5.22	5.61	5.28	5.62	5.28	5.63
avg	4.80	5.45	4.80	5.45	5.04	5.47	5.03	5.48	4.79	5.44	4.79	5.44	5.02	5.46	5.00	5.46

Table 8: Estimated effects for DIP_{eq} from the 2^4 FFD, by Yates's analysis

Run #	DIP_{eq}* (kg)	I	II	III	IV	divisor	Effect IV/divisor	Identity of effects
1	4.800286	10.247113	20.499169	41.516841	82.912298	16	5.18	average
2	5.446827	10.252056	21.017672	41.395457	4.374556	8	0.55	$(\tau\alpha)_{eff}$
3	4.799894	10.514967	20.458782	2.179211	-0.013578	8	-1.70E-03	m_m
4	5.452162	10.502705	20.936675	2.195345	0.055916	8	6.99E-03	$(\tau\alpha)_{eff}\, m_m$
5	5.043170	10.226370	1.298809	-0.007319	0.996396	8	0.12	U_2
6	5.471797	10.232412	0.880402	-0.006259	-0.816562	8	-0.10	$(\tau\alpha)_{eff}\, U_2$
7	5.025465	10.474488	1.296750	0.028875	-0.035548	8	-4.44E-03	$m_m\, U_2$
8	5.477240	10.462187	0.898595	0.027041	0.035274	8	4.41E-03	$(\tau\alpha)_{eff}\, m_m\, U_2$
9	4.790146	0.646541	0.004943	0.518503	-0.121384	8	-1.52E-02	A_4
10	5.436224	0.652268	-0.012262	0.477893	0.016134	8	2.02E-03	$(\tau\alpha)_{eff}\, A_4$
11	4.790870	0.428627	0.006042	-0.418407	0.001060	8	1.32E-04	$m_m\, A_4$
12	5.441542	0.451775	-0.012301	-0.398155	-0.001834	8	-2.29E-04	$(\tau\alpha)_{eff}\, m_m\, A_4$
13	5.018207	0.646078	0.005727	-0.017205	-0.040610	8	-5.08E-03	$U_2\, A_4$
14	5.456281	0.650672	0.023148	-0.018343	0.020252	8	2.53E-03	$(\tau\alpha)_{eff}\, U_2\, A_4$
15	5.000833	0.438074	0.004594	0.017421	-0.001138	8	-1.42E-04	$m_m\, U_2\, A_4$
16	5.461354	0.460521	0.022447	0.017853	0.000432	8	5.40E-05	$(\tau\alpha)_{eff}\, m_m\, U_2\, A_4$

** Average values calculated for the 20-day period considered.*

Table 9: Determination of Steepest Ascent runs

	$(\tau\alpha)_{eff}$	m_m (kg)	U_2 (W m^{-2} K^{-1})	A_4 (m^2)
Lower level	0.50	10	4	2
Upper level	0.80	50	200	10
Mean level	0.65	30	102	6
Increment, Δz_j	0.15	20	98	4
Coefficient, b_j (see "Effect" in Tab. 8)	5.47E-01	–1.70E-03	1.25E-01	–1.52E-02
$\Delta z_j\, b_j$	8.20E-02	–3.39E-02	1.22E+01	–6.07E-02
Step, $\frac{\Delta z_j b_j}{max(b_j)}$	0.150	–0.062	22.322	–0.111
Normalized step= Step/3	0.050	–0.021	7.441	–0.037
Runs for optimization:				
SA1	0.70	29.98	109.4	5.96
SA2	0.75	29.96	116.9	5.93
SA3	0.80	29.94	124.3	5.89
SA4	0.85	29.92	131.8	5.85
SA5	0.90	29.90	139.2	5.82
Fixed values:	–	30	–	6

Table 10: Results of Steepest Ascent runs, for DIP_{eq} (kg)

May 2005 day	SA1	SA2	SA3	SA4	SA5
3	5.22	5.28	5.32	5.36	5.40
4	5.37	5.43	5.47	5.52	5.56
5	5.33	5.39	5.44	5.49	5.52
6	5.06	5.12	5.18	5.24	5.28
7	5.41	5.46	5.50	5.54	5.57
8	5.38	5.43	5.49	5.52	5.56
9	5.45	5.51	5.55	5.58	5.61
10	5.50	5.55	5.58	5.61	5.67
11	5.48	5.52	5.55	5.59	5.68
12	5.44	5.49	5.52	5.56	5.64
13	5.32	5.37	5.42	5.46	5.51
14	5.15	5.21	5.26	5.31	5.35
15	5.40	5.44	5.49	5.52	5.54
16	5.43	5.48	5.51	5.55	5.68
17	5.56	5.60	5.63	5.67	5.74
18	5.43	5.46	5.49	5.52	5.63
19	5.42	5.46	5.49	5.53	5.61
20	5.34	5.38	5.41	5.44	5.56
21	5.43	5.47	5.50	5.53	5.64
22	5.37	5.41	5.44	5.47	5.60
min	5.06	5.12	5.18	5.24	5.28
max	5.56	5.60	5.63	5.67	5.74
avg	5.37	5.42	5.46	5.50	5.57

FIGURE CAPTIONS

Figure 1: Scheme of the adsorptive ice-maker.

Figure 2: Ambient temperature and solar radiation recorded in May 2005.

Figure 3: Average *COPs*, *UE*, *DIP* and DIP_{eq} calculated for the FFD 16 runs (the lines are used only as an eye-guide).

Figure 4: Calculated values of DIP_{eq} for odd (a) and even (b) FFD runs in the investigated period (the lines are used only as an eye-guide).

Figure 5: Main effects and interactions for DIP_{eq} calculated from the FFD.

Figure 6: Two-way table for the $(\tau\alpha)_{eff}$ U_2 interaction.

Figure 7: Adsorbent material and condenser temperature calculated for the investigated period and the optimized ice-maker (i.e., case with $(\tau\alpha)_{eff}$ =0.9, U_2=139.2 W m^{-2} K^{-1}, m_m=30 kg and A_4=6 m^2).

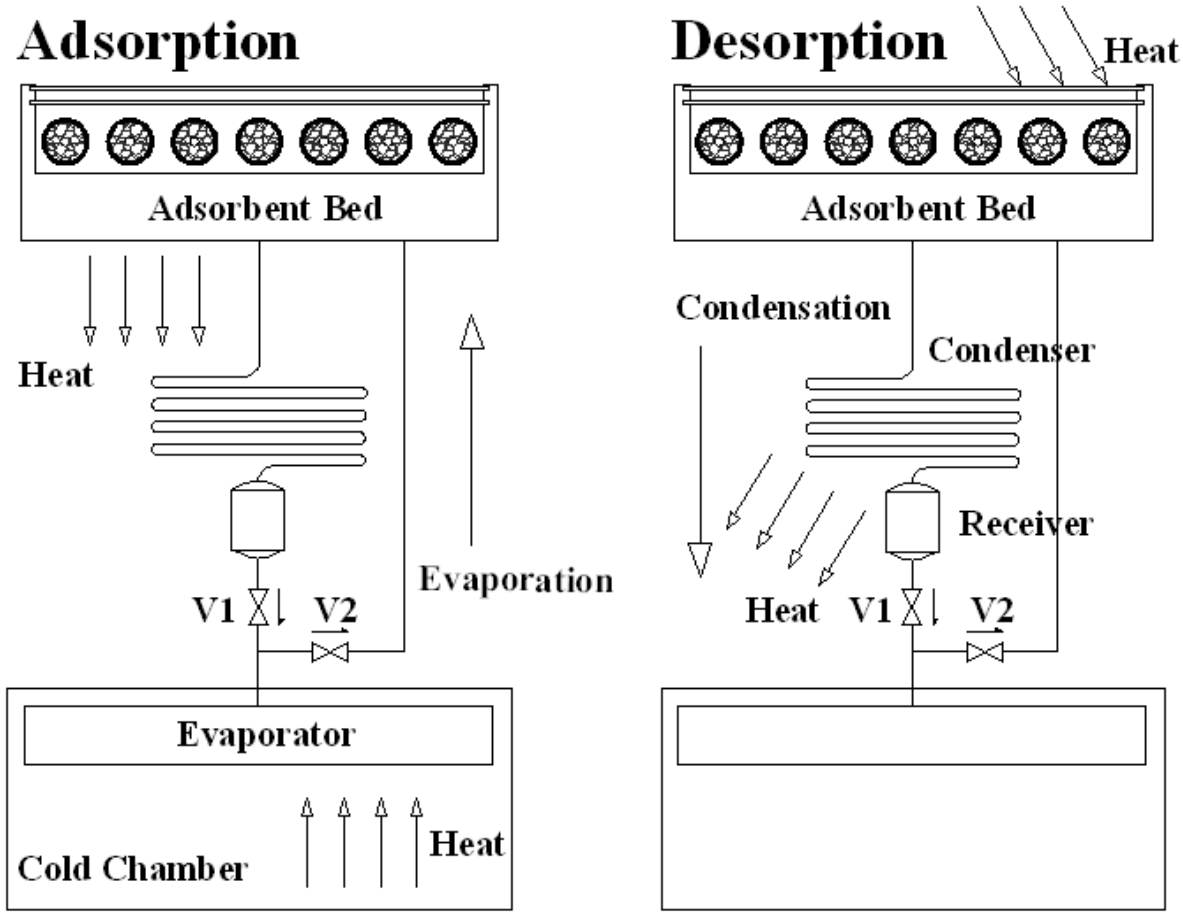
Adsorption
Adsorbent Bed
Heat
V1
V2
Evaporation
Evaporator
Cold Chamber
Heat
Desorption
Heat
Adsorbent Bed
Condensation
Condenser
Receiver
Heat
V1
V2

Figure 1

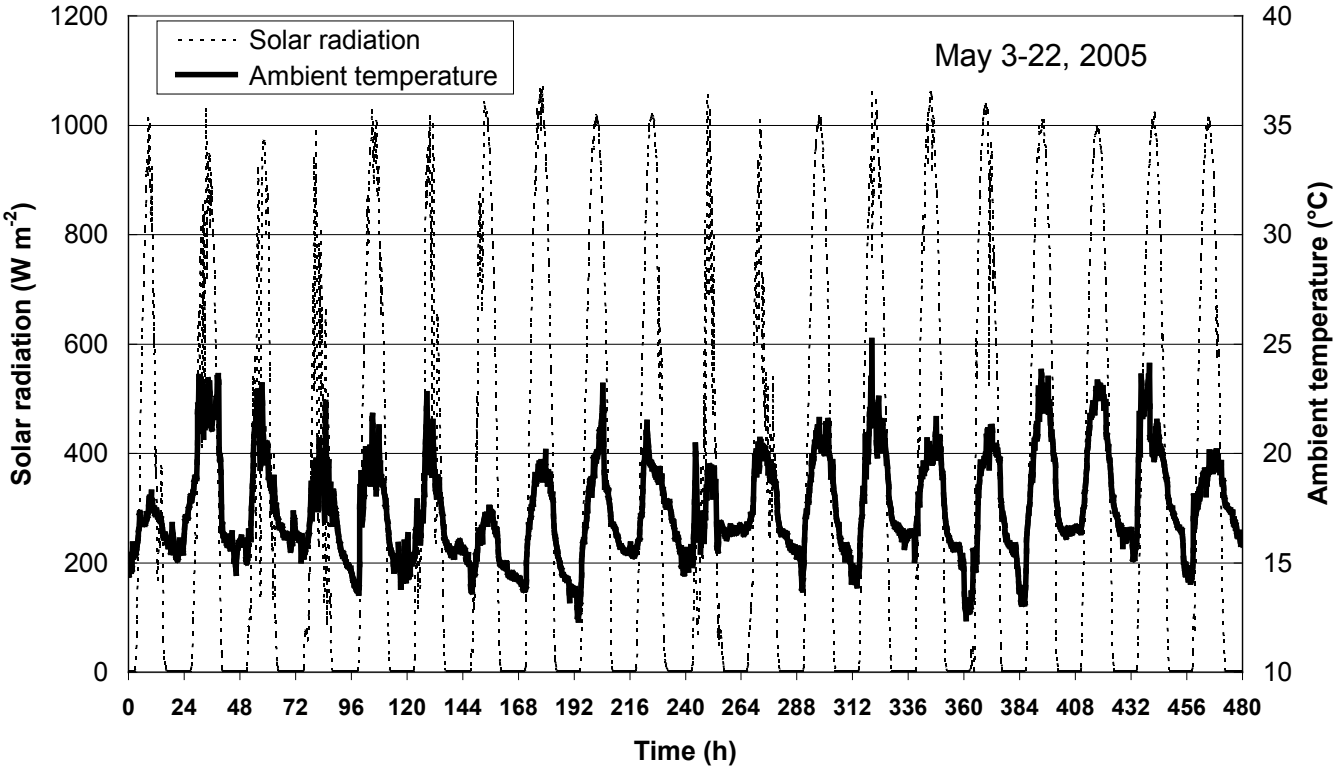
Solar radiation
Ambient temperature
May 3-22, 2005
Solar radiation (W m-2)
Ambient temperature (°C)
Time (h)
1200
1000
800
600
400
200
0
40
35
30
25
20
15
10
0 24 48 72 96 120 144 168 192 216 240 264 288 312 336 360 384 408 432 456 480

Figure 2

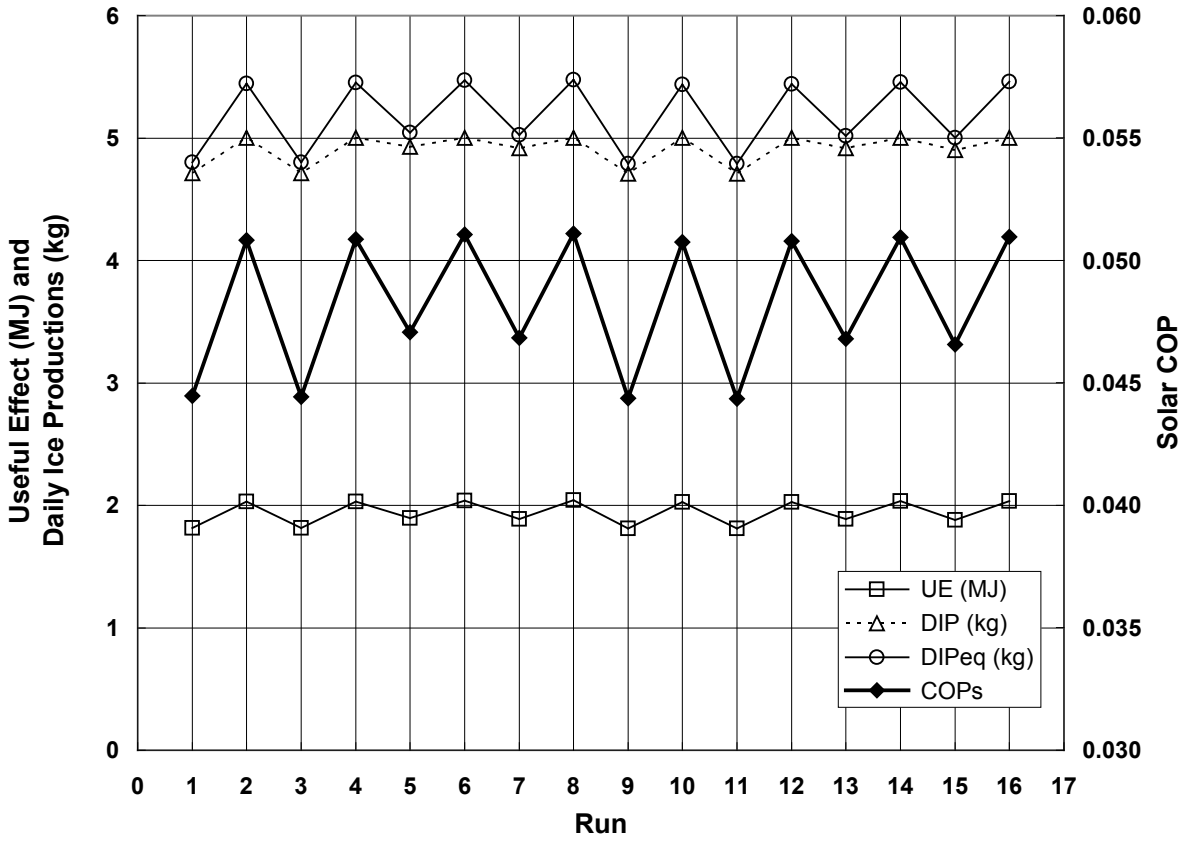
Useful Effect (MJ) and
Daily Ice Productions (kg)
Solar COP
Run
UE (MJ)
DIP (kg)
DIPeq (kg)
COPs
0
1
2
3
4
5
6
0.030
0.035
0.040
0.045
0.050
0.055
0.060
0
1
2
3
4
5
6
7
8
9
10
11
12
13
14
15
16
17

Figure 3

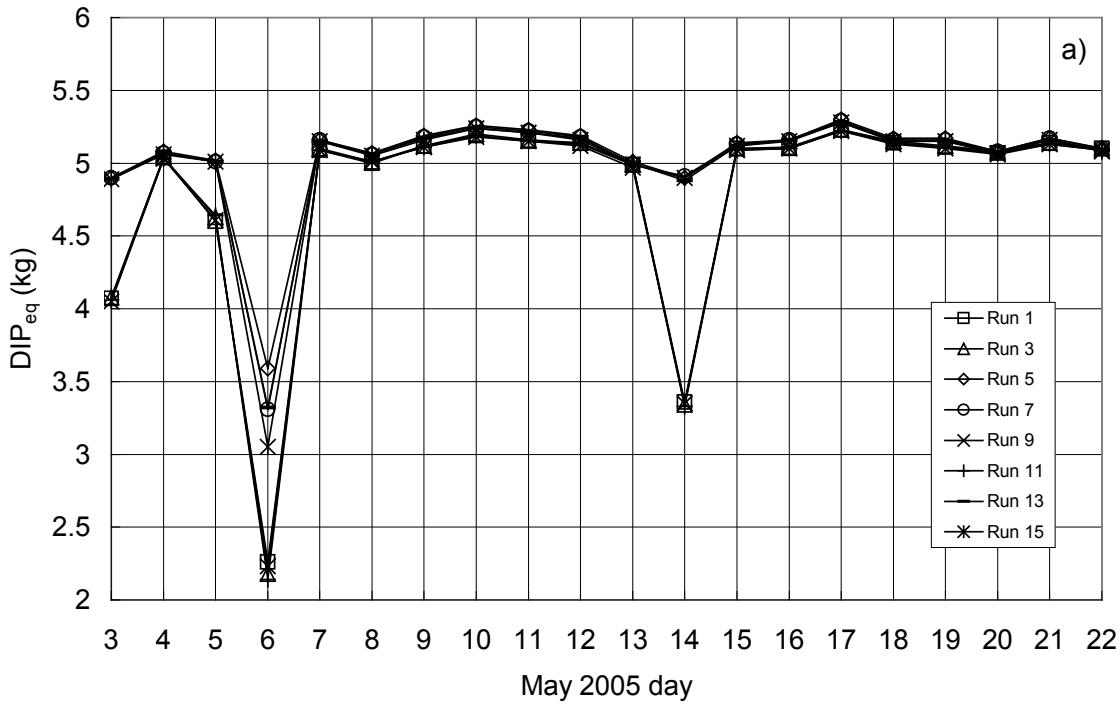
a)
DIP$_{eq}$ (kg)
6
5.5
5
4.5
4
3.5
3
2.5
2
3 4 5 6 7 8 9 10 11 12 13 14 15 16 17 18 19 20 21 22
May 2005 day
Run 1
Run 3
Run 5
Run 7
Run 9
Run 11
Run 13
Run 15

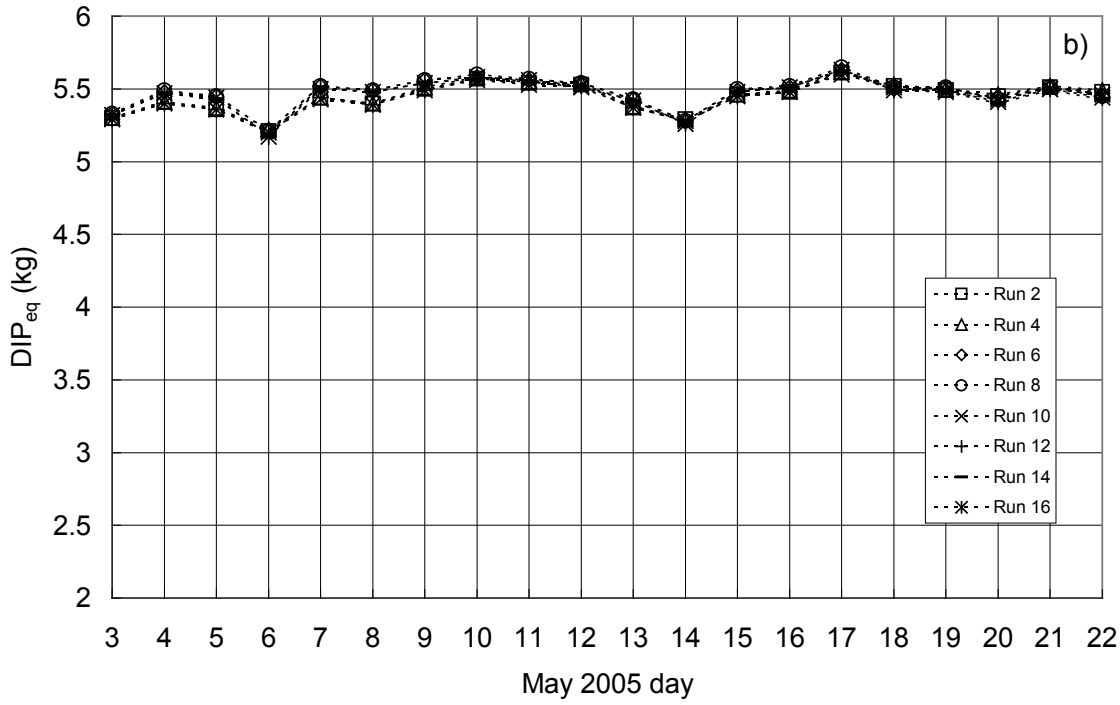
b)
DIP$_{eq}$ (kg)
6
5.5
5
4.5
4
3.5
3
2.5
2
3 4 5 6 7 8 9 10 11 12 13 14 15 16 17 18 19 20 21 22
May 2005 day
Run 2
Run 4
Run 6
Run 8
Run 10
Run 12
Run 14
Run 16

Figure 4

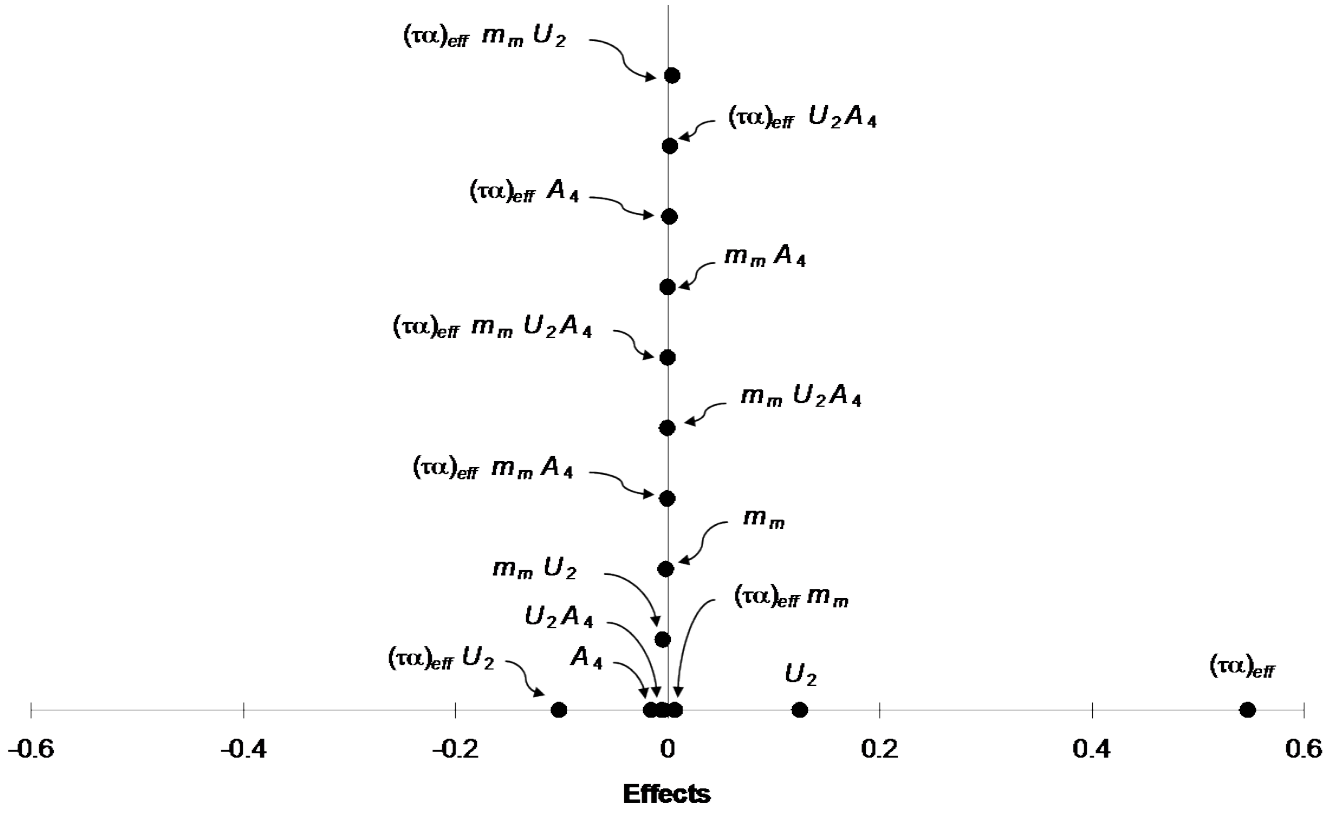
$(\tau\alpha)_{eff}\ m_m\ U_2$
$(\tau\alpha)_{eff}\ U_2A_4$
$(\tau\alpha)_{eff}\ A_4$
$m_m\ A_4$
$(\tau\alpha)_{eff}\ m_m\ U_2A_4$
$m_m\ U_2A_4$
$(\tau\alpha)_{eff}\ m_m\ A_4$
m_m
$m_m\ U_2$
$(\tau\alpha)_{eff}\ m_m$
U_2A_4
$(\tau\alpha)_{eff}\ U_2$
A_4
U_2
$(\tau\alpha)_{eff}$
-0.6
-0.4
-0.2
0
0.2
0.4
0.6
Effects

Figure 5

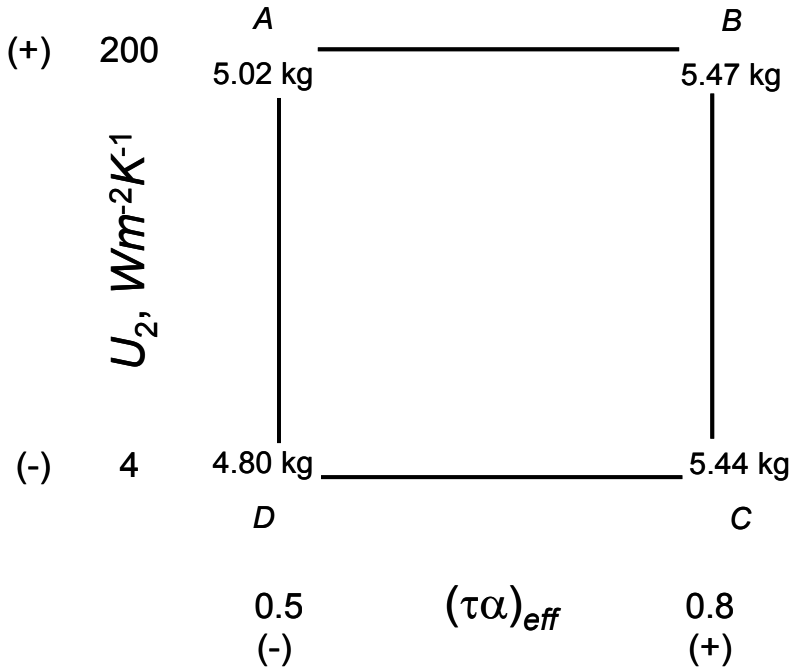
A
B
(+)
200
5.02 kg
5.47 kg
U_2, $Wm^{-2}K^{-1}$
(-)
4
4.80 kg
5.44 kg
D
C
0.5
$(\tau\alpha)_{eff}$
0.8
(-)
(+)

Figure 6

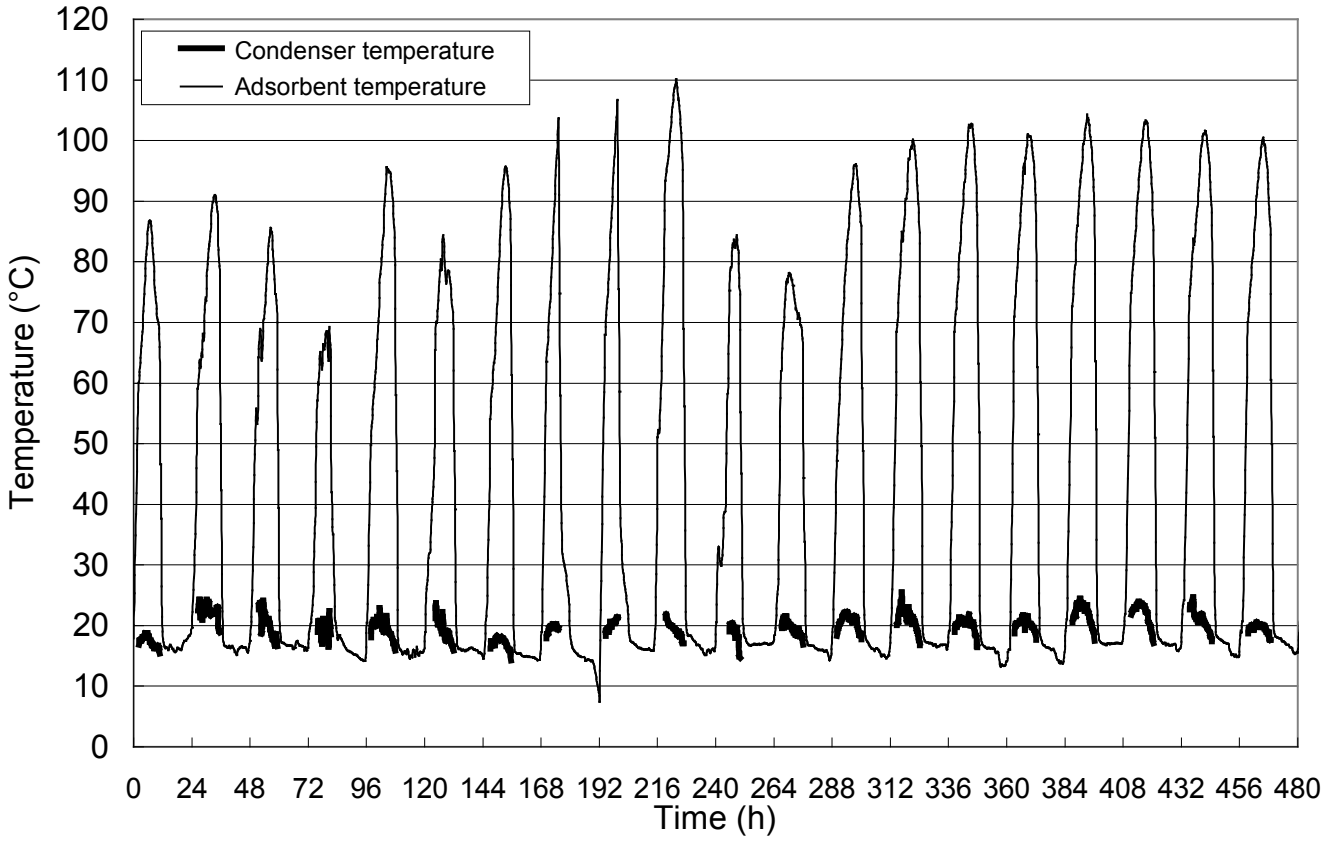
Condenser temperature
Adsorbent temperature
Temperature (°C)
120
110
100
90
80
70
60
50
40
30
20
10
0
0 24 48 72 96 120 144 168 192 216 240 264 288 312 336 360 384 408 432 456 480
Time (h)

Figure 7